IEEE Access
Multidisciplinary | Rapid Review | Open Access Journal

Received July 2, 2019, accepted July 20, 2019, date of publication July 25, 2019, date of current version August 13, 2019.

Digital Object Identifier 10.1109/ACCESS.2019.2931118

Stability Evaluation on the Droop Controller Parameters of Multi-Terminal DC Transmission Systems Using Small-Signal Model

YANBO CHE[1], JINGJING JIA[1], JIEBEI ZHU[1], XIALIN LI[1], ZIHAN LV[1], AND MING LI[2]
[1]Key Laboratory of Smart Grid of Ministry of Education, Tianjin University, Tianjin 300072, China
[2]College of Computer, Qinghai Nationalities University, Xining 810007, China

Corresponding author: Jiebei Zhu (zhujiebei@hotmail.com)

This work was supported by the Basic Research Program of Qinghai Province, China, under Grant 2018-ZJ-764.

ABSTRACT For a complex multi-terminal DC (MTDC) transmission system, controller parameter settings exert tremendous influence on the system dynamics and transient stability. The traditional droop control scheme, which aims to locally control the converter's power by regulating its DC voltage according to the pre-defined droop slopes, does not normally employ communications for coordination with other terminals. The droop scheme is designed for power sharing purpose and its controller gains' impact on the MTDC network voltage is usually ignored. Moreover, the droop controller parameters are selected without considering various operating states of the MTDC terminals. This paper proposes a droop controller parameters select the criterion to cater to MTDC network voltage stability. To do so, a detailed small-signal model for a four-terminal MTDC system candidate with typical network topology, considering each converter station's electrical characteristics and cascaded control loops, is established. In order to maintain the fidelity for DC network modeling, the model also takes account of the DC network electrical dynamics and losses. A time-domain simulation model is built in Matlab Simulink to verify the correctness of the small-signal model.

INDEX TERMS Droop control, small signal analysis, stability, VSC-MTDC.

I. INTRODUCTION

The new-generation technology of flexible Voltage-Source-Converter-based (VSC) high-voltage direct current (HVDC) transmission system compared to conventional Line-Commutated-Converter-based (LCC) HVDC technology brings new opportunity of fast power control and independent multi-terminal operations [1]. With the existing trend of MTDC being expanded to possess more terminals and DC circuits, the structural complexity of the future MTDC system will dramatically grow, and oscillation problems have been frequently observed as reported in [2]–[4]. The occurrence of oscillation will lead to DC voltage oscillation, and even cause the outage of converter station. In order to avoid power or DC voltage fluctuations, control parameters of MTDC system shall be considered in the steady and dynamic-state stability [5], [6]. Therefore, to solve this problem, it is technically necessary to obtain its mathematical model and evaluate its stability problems. One of the widely accepted issues is the stability of the entire MTDC voltage as a prior control objective. Reasonable selection of converter parameters may effectively improve the damping characteristics of the system and reduce the risks of operational oscillation or failure.

Time-domain simulation may assist with MTDC controller gain selection. However, for a large-scale MTDC system with significant controller interactions, the MTDC model is gone complex and it is subject to all-round contingency analysis, simulation speed & accuracy constraints due to large computation load. In addition, in multi-terminal systems, as operating conditions of external converter stations change or dynamic interactions among subsystems take place, the most ideal controller gain may deviate and considerable effort can be spent to evaluate the controller gains and identify right ones.

Small signal stability analysis (SSSA) for VSC-MTDC system is usually carried out instead of time-domain

The associate editor coordinating the review of this manuscript and approving it for publication was Feiqi Deng.

simulation [5]–[14], which mainly falls into two categories with different emphasis for VSC systems: SSSA on the converter control system [12]–[20] itself including the influence of PLL and AC system strength [9], [10], and SSSA on the system-wide stability (e.g. system stability with multiple VSC integrations [11]). An SSSA model for Modular Multilevel Converter (MMC) including capacitance energy and circulating current of sub-modules is established in [12] to analyze the internal parameters, but the application in the overall dynamics of HVDC has not been developed. An SSSA model for SC rectifier and inverter systems connected to weak networks is utilized for developing an improved reactive power control method in [13]. The main state variables affecting the dominant poles are analyzed by the derived participation factor matrix but further research is needed to verify the applicability of the improved reactive power control method. In reference [10], a VSC small signal model with PLL is proposed to quantitatively study the influence of power system impedance and PLL parameters on dynamic and stability limits. However, the analysis only focuses on the stability of a single VSC connected AC system whereas the interactions among multi-terminal are not included. A four-terminal network connecting wind farm and grid side VSCs without considering DC network dynamics is modeled in state space in [14], and the stable operation ranges of VSC control parameters is studied by calculating the eigenvalue.

The main objective of MTDC control scheme is to maintain the DC voltage stability and power balance of the system on top of ensuring the safe and stable operation of individual converter stations [15]. DC voltage droop control tries to control DC voltage to its reference level while at the same time contributing some balancing power [16]. Since the two actions are somewhat contradicting that one action happens at the cost of steady state deviations for the other. To analyze the influence of voltage droop coefficient on power distribution, the Jacobian matrix of power to voltage is derived in [16], and the essential relationship between DC voltage change and power change in converter station is revealed, but no parameter sensitivity analysis is performed. Reference [17] compares the effects of different control strategies and control parameters on the stability of the system, and concludes that DC voltage droop control is superior to master-slave control in terms of the eigenvalue analysis of the performance of the two control schemes. Reference [18] studied the DC voltage and power dispatch under different operational conditions and proposed different DC grid management strategies. The research shows the robust performance of the proposed system by switching the control modes, but small perturbation stability regarding to the controller parameter optimization is not discussed. A MTDC droop control strategy considering transmission losses and renewable energy fluctuations is proposed in [19], where the droop coefficient is selected by assessing the relationship between DC voltage and its reference. Nevertheless, the simulation is carried out under the condition of large disturbance. An adaptive decentralized droop controller is proposed to schedule the transient droop coefficient by the SSSA on power sharing mechanism in [20]. However, the proposed control scheme is applicable to the micro-grid scenarios.

Although the DC voltage droop control schemes in MTDC has been explored in the aforementioned literature, the impact of DC voltage droop controller parameters on the DC grid voltage stability has not been well addressed. To study the effect of droop controller parameters on the small signal stability of DC voltage when power flow dynamics exist in MTDC system, it is necessary to derive a detailed accurate small signal model including individual VSC control modes and the DC network characteristics. In this paper, a complete small signal mathematical model of four-terminal MTDC system is established by linearizing all state equations at a certain point of operation, so as to carry out SSSA. The inductance parameter of DC cable is considered to make the results more convincing. The parameters of the droop controller are analyzed and selected through the observation on the distributions of zeros and poles in root locus chart, which is more obvious and intuitive than previous works in [14]. The accuracy of the developed model is verified by comparing with the simulation results in time-domain.

The organization of this paper is as follows: Section II presents the MTDC system structure and the small signal model of the overall system. In Section III, the accuracy of small signal model is verified. Simulations are carried out to analyze the influence of parameters on system stability in Section IV. Section V carries out time-domain simulations verification on the impact of control parameters. Conclusions are drawn in Section VI.

II. SYSTEM CONFIGURATION AND MODELING

A. SYSTEM STRUCTURE

A four-terminal candidate MTDC system is illustrated in Fig. 1, where converter stations are connected in parallel star mode and their power flow direction are indicated. Both wind farm-side voltage source converter (WFVSC) station 2 and 4 work in input state with respect to the DC grid, and adopt droop control mode and constant DC bus voltage control mode respectively. Whereas grid-side voltage source converter (GSVSC) station 1 and 3 work in output state, and adopt constant active power control mode.

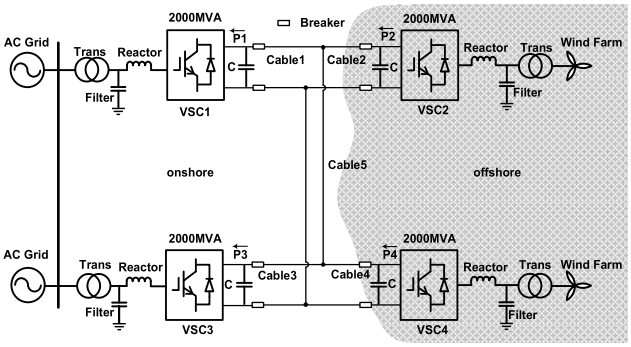

FIGURE 1. The candidate four-terminal DC system.

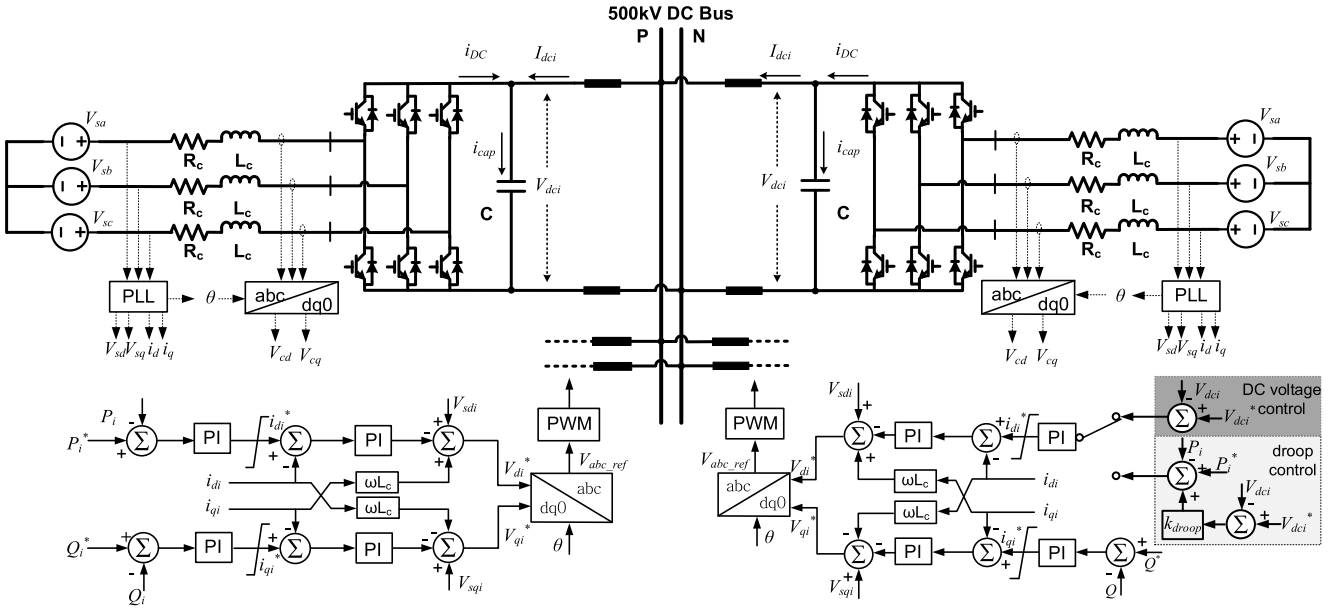

FIGURE 2. Control systems for WFVSCs and GSVSCs.

Each AC source is represented by a Thevenin impedance model consisting of R_S and L_S. Each VSC is represented by its average model, with its AC side by three controlled voltage sources only considering the fundamental frequency, and its DC side is represented by a controlled current source.

B. WFVSC SUBSYSTEM MODELING

Three-phase AC voltage and current at the points of common coupling (PCC) are measured as the inputs into individual VSC control systems. As seen from Fig. 1, after Park transformation the dynamic equations for each VSC in the *dq* rotating reference frame are given as follow on the basis of Kirchhoff's law:

$$L_c \frac{di_{di}}{dt} = -V_{cdi} + V_{sdi} - R_c i_{di} + \omega L_c i_{qi} \tag{1}$$

$$L_c \frac{di_{qi}}{dt} = -V_{cqi} + V_{sqi} - R_c i_{qi} - \omega L_c i_{di} \tag{2}$$

where L_c and R_c are the total equivalent inductance and resistance of AC side (including phase reactor and interface transformer); ω is synchronous frequency of the AC system; i_{di} and i_{qi} are ac system *dq* frame currents; V_{sdi} and V_{sqi} are the ac system *dq* frame voltages; V_{cdi} and V_{cqi} are *dq* frame voltages at AC side of VSC and i is the reference number of converter stations. Assuming that the converter stations are lossless, the current flowing through the capacitor can be expressed as:

$$C\frac{dV_{dci}}{dt} = \frac{P_i}{V_{dci}} - I_{dci} = \frac{V_{cdi}i_{di} + V_{cqi}i_{qi}}{V_{dci}} - I_{dci} \tag{3}$$

where C is the capacitance on the DC side of VSC; V_{dci} is the DC voltage; P_i is the active power of the VSC; I_{dci} is the current on the dc transmission line.

As shown in Fig. 2, the control systems for WFVSCs are applied with different control modes while one terminal (VSC4) adopts DC voltage control and the other (VSC2) adopts droop control [21]. A phase-locked loop is required for orienting the converter controllers with the grid angle. Hierarchical control strategy with a fast inner current controller and the slower outer DC link voltage-power droop controller, hereafter simply referred as droop controller, is shown in Fig. 2. The inner current control loop is realized in *dq* reference frame aligned with PCC voltage based on the equations across the reactor given as follows:

$$\begin{aligned} V_{cdi} &= V_{sdi} + \omega L i_{qi} - [k_p(i_{di}^* - i_{di}) + k_i z_{1i}] \\ V_{cqi} &= V_{sqi} - \omega L i_{di} - [k_p(i_{qi}^* - i_{qi}) + k_i z_{2i}] \end{aligned} \tag{4}$$

where k_p and k_i represent the proportional and integral (PI) gains of the inner loop current controller, respectively; auxiliary variables z_{1i} and z_{2i} represent the integral parts of inner loop controller, with

$$\begin{aligned} z_{1i} &= \int (i_d^* - i_d)dt \\ z_{2i} &= \int (i_q^* - i_q)dt \end{aligned} \tag{5}$$

All the current controllers have the same PI gains to make the analysis more clearly.

From Fig. 2, the DC voltage droop controller and reactive power controller are implemented by PI regulators. The reference currents of the inner loop i_{di}^* and i_{qi}^* can be obtained from the outer loop controllers as:

$$\begin{aligned} i_{di}^* &= k_{pv}\left[k_{droop}(V_{dci}^* - V_{dci}) + (P_i^* - P_i)\right] + k_{iv} z_{3i} \\ i_{qi}^* &= k_{pq}(Q_i^* - Q_i) + k_{iq} z_{4i} \end{aligned} \tag{6}$$

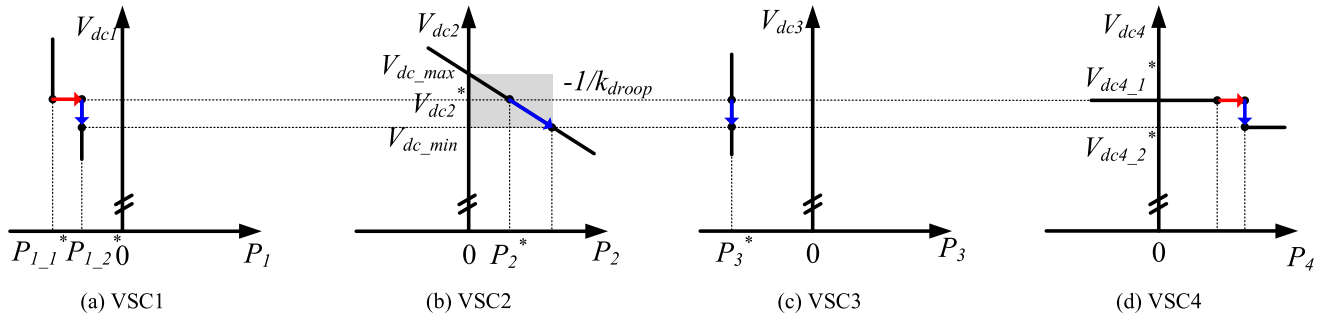

FIGURE 3. DC voltage droop control configuration and corresponding characteristic.

where, k_{pv} and k_{iv} represent the proportional and integral gains of the DC voltage outer loop controller, respectively; k_{pq} and k_{iq} represent the proportional and integral gains of the reactive power outer loop controller, respectively; P_i and Q_i are the active and reactive power of the converters; V_{dci}^*, P_i^*, and Q_i^* are the reference values; z_{3i} and z_{4i} are auxiliary variables defined to represent the integral parts of outer loop controllers with

$$z_{3i} = \int \left[k_{droop}\left(V_{dci}^* - V_{dci}\right) + \left(P_i^* - P_i\right)\right] dt$$
$$z_{4i} = \int \left(Q_i^* - Q_i\right) dt \tag{7}$$

k_{droop} is the droop coefficient and $-1/k_{droop}$ represents the slope of the curve in Fig. 3(b).

Fig. 3 shows the DC voltage versus active power characteristic curves for the four VSCs when power step change and DC voltage step change occurs, respectively. And according to Fig. 3, the droop slope can be represented as:

$$-\frac{1}{k_{droop}} = -\frac{V_{dc2\_\max} - V_{dc2}^*}{P_2^*} \tag{8}$$

where V_{dc_max} refers to the upper limit value of the DC voltage and V_{dc2}^* and P_2^* refer to the rated voltage and rated active power of VSC_2.

The active and reactive power of the four converter stations can be expressed as

$$P_i = V_{sdi}i_{di} + V_{sqi}i_{qi}$$
$$Q_i = V_{sdi}i_{qi} - V_{sqi}i_{di} \tag{9}$$

Utilizing Taylor series with the higher-order terms neglected [14], [22], the linearized form of (9) is expressed as:

$$\Delta P_i = i_{di}\Delta V_{sdi} + i_{qi}\Delta V_{sqi} + V_{sdi}\Delta i_{di} + V_{sqi}\Delta i_{qi}$$
$$\Delta Q_i = i_{qi}\Delta V_{sdi} - i_{di}\Delta V_{sqi} + V_{sdi}\Delta i_{qi} - V_{sqi}\Delta i_{di} \tag{10}$$

After linearization of (1), (2) and (3), by substituting (4)-(7) and (10) the linearized models of VSC are expressed as:

$$\frac{d\Delta i_{di}}{dt} = -\frac{k_p + R_c + k_pk_{pv}v_{sdi}}{L_c}\Delta i_{di} - \frac{k_pk_{pv}v_{sqi}}{L_c}\Delta i_{qi} - \frac{k_pk_{pv}k_{droop}}{L_c}\Delta V_{dci} + \frac{k_i}{L_c}\Delta z_{1i} + \frac{k_pk_{iv}}{L_c}\Delta z_{3i} - \frac{k_pk_{pv}i_{di}}{L_c}\Delta v_{sdi} - \frac{k_pk_{pv}i_{qi}}{L_c}\Delta v_{sqi} + \frac{k_pk_{pv}k_{droop}}{L_c}\Delta V_{dci}^* + \frac{k_pk_{pv}}{L_c}\Delta P_i^*$$

$$\frac{d\Delta i_{qi}}{dt} = \frac{k_pk_{pq}v_{sqi}}{L_c}\Delta i_{di} - \frac{k_pk_{pq}v_{sdi} + k_p + R_c}{L_c}\Delta i_{qi} + \frac{k_i}{L_c}\Delta z_{2i} + \frac{k_pk_{iq}}{L_c}\Delta z_{4i} - \frac{k_pk_{pq}i_{qi}}{L_c}\Delta v_{sdi} + \frac{k_pk_{pq}i_{di}}{L_c}\Delta v_{sqi} + \frac{k_pk_{pq}}{L_c}\Delta Q_i^*$$

$$\frac{d\Delta V_{dci}}{dt} = \frac{v_{cdi} + k_pi_{di} + k_pk_{pv}i_{di}v_{sdi} - \omega L_ci_{qi} - k_pk_{pq}i_{qi}v_{sqi}}{CV_{dci}}\Delta i_{di} + \frac{v_{cqi} + k_pi_{qi} + \omega Li_{di} + k_pk_{pv}i_{di}v_{sq} + k_pk_{pq}i_{qi}v_{sdi}}{CV_{dci}}\Delta i_{qi} + [-\frac{(v_{cdi}i_{di}+v_{cqi}i_{qi})}{CV_{dci}^2} + \frac{k_pk_{pv}k_{droop}i_{di}}{CV_{dci}}]\Delta V_{dci} - \frac{k_ii_{di}}{CV_{dci}}\Delta z_{1i} - \frac{k_ii_{qi}}{CV_{dci}}\Delta z_{2i} - \frac{k_pk_{iv}i_{di}}{CV_{dci}}\Delta z_{3i} - \frac{k_pk_{iq}i_{qi}}{CV_{dci}}\Delta z_{4i} + (\frac{k_pk_{pv}i_{di}^2}{CV_{dci}} + \frac{k_pk_{pq}i_{qi}^2}{CV_{dci}})\Delta v_{sdi} + \frac{k_pk_{pv}i_{di}i_{qi} + i_{qi} - k_pk_{pq}i_{di}i_{qi}}{CV_{dci}}\Delta v_{sqi} - \frac{1}{C}\Delta I_{dci} - \frac{k_pk_{pv}k_{droop}i_{di}}{CV_{dci}}\Delta V_{dci}^* - \frac{k_pk_{pv}i_{di}}{CV_{dci}}\Delta P_i^* - \frac{k_pk_{pq}i_{qi}}{CV_{dci}}\Delta Q_i^* \tag{11}$$

To reduce the order, the output of each integrator is differentiated. By substituting formula (6) and (10), formula (12) is derived from formula (5) and (7), so the linearized forms of the auxiliary variables z_{1i} to z_{4i} are:

$$\frac{d\Delta z_{1i}}{dt} = \Delta i_{di}^* - \Delta i_{di} = -(k_{pv}v_{sdi} + 1)\Delta i_{di} - k_{pv}v_{sqi}\Delta i_{qi} - k_{pv}k_{droop}\Delta V_{dci} + k_{iv}\Delta z_{3i} - k_{pv}i_{di}\Delta v_{sdi} k_{pv}i_{qi}\Delta v_{sqi} + k_{pv}k_{droop}\Delta V_{dci}^* + k_{pv}\Delta P_i^*$$

$$\frac{d\Delta z_{2i}}{dt} = \Delta i_{qi}^* - \Delta i_{qi} = k_{pq}v_{sqi}\Delta i_{di} - (k_{pq}v_{sdi} + 1)\Delta i_{qi} + k_{iq}\Delta z_{4i} - k_{pq}i_{qi}\Delta v_{sdi} + k_{pq}i_{di}\Delta v_{sqi} + k_{pq}\Delta Q_i^*$$

$$\frac{d\Delta z_{3i}}{dt} = k_{droop}\Delta V_{dci}^* - k_{droop}\Delta V_{dci} + \Delta P_i^* - \Delta P_i$$

$$= -v_{sdi}\Delta i_{di} - v_{sqi}\Delta i_{qi} - k_{droop}\Delta V_{dci} - i_{di}\Delta v_{sdi} - i_{qi}\Delta v_{sqi} + k_{droop}\Delta V^*_{dci} + \Delta P^*_i$$

$$\frac{d\Delta z_{4i}}{dt} = \Delta Q^*_i - \Delta Q_i = \Delta Q^*_i + v_{sqi}\Delta i_{di} - v_{sdi}\Delta i_{qi} - i_{qi}\Delta v_{sdi} + i_{di}\Delta v_{sqi}. \quad (12)$$

C. GSVSC SUBSYSTEM MODELING

Fig. 2 shows the equivalent circuit of grid side converters systems and the direction of DC current is specified which is different from that of the wind farm side VSCs. The linearized model of the grid side converters VSC_1 and VSC_3 is:

$$C\frac{dV_{dci}}{dt} = \frac{P_i}{V_{dci}} + I_{dci} = \frac{V_{cdi}i_{di} + V_{cqi}i_{qi}}{V_{dci}} + I_{dci} \quad (13)$$

The inner loop control is the same as that of the WFVSCs, but the outer loop d-axis control mode adopts constant active power control which is different from DC voltage droop control. The reference values of inner loop in dq frame can be obtained by controlling active and reactive power as follows:

$$i^*_{di} = k_{pp}(P^*_i - P_i) + k_{ip}z_{3i}$$
$$i^*_{qi} = k_{pq}(Q^*_i - Q_i) + k_{iq}z_{4i} \quad (14)$$

where k_{pp} and k_{ip} represent the proportional and integral gains of active power controller, respectively; z_{3i} and z_{4i} represent the integral parts of the outer loop regulator shown as follow:

$$z_{3i} = \int \left[\left(P^*_i - P_i\right)\right] dt$$
$$z_{4i} = \int \left(Q^*_i - Q_i\right) dt \quad (15)$$

The linearized models of the VSC_1 and VSC_3 in the dq coordinates are:

$$\frac{d\Delta i_{di}}{dt} = -\frac{k_p + R_c + k_pk_{pp}v_{sdi}}{L_c}\Delta i_{di} - \frac{k_pk_{pp}v_{sqi}}{L_c}\Delta i_{qi} + \frac{k_i}{L_c}\Delta z_{1i} + \frac{k_pk_{ip}}{L_c}\Delta z_{3i} - \frac{k_pk_{pp}i_{di}}{L_c}\Delta v_{sdi} - \frac{k_pk_{pp}i_{qi}}{L_c}\Delta v_{sqi} + \frac{k_pk_{pp}}{L_c}\Delta P^*_i$$

$$\frac{d\Delta i_{qi}}{dt} = \frac{k_pk_{pq}v_{sqi}}{L_c}\Delta i_{di} - \frac{k_pk_{pq}v_{sdi} + k_p + R_c}{L_c}\Delta i_{qi} + \frac{k_i}{L_c}\Delta z_{2i} + \frac{k_pk_{iq}}{L_c}\Delta z_{4i} - \frac{k_pk_{pq}i_{qi}}{L_c}\Delta v_{sdi} + \frac{k_pk_{pq}i_{di}}{L_c}\Delta v_{sqi} + \frac{k_pk_{pq}}{L_c}\Delta Q^*_i$$

$$\frac{d\Delta V_{dci}}{dt} = \frac{v_{cdi} + k_pi_{di} + k_pk_{pp}i_{di}v_{sdi} - \omega L_ci_{qi} - k_pk_{pq}i_{qi}v_{sqi}}{CV_{dci}}\Delta i_{di} + \frac{v_{cqi} + k_pi_{qi} + \omega Li_{di} + k_pk_{pp}i_{di}v_{sq} + k_pk_{pq}i_{qi}v_{sdi}}{CV_{dci}}\Delta i_{qi} - \frac{(v_{cdi}i_{di} + v_{cqi}i_{qi})}{CV^2_{dci}}\Delta V_{dci} - \frac{k_ii_{di}}{CV_{dci}}\Delta z_{1i} - \frac{k_ii_{qi}}{CV_{dci}}\Delta z_{2i} - \frac{k_pk_{ip}i_{di}}{CV_{dci}}\Delta z_{3i} - \frac{k_pk_{iq}i_{qi}}{CV_{dci}}\Delta z_{4i} + \left(\frac{i_d + k_pk_{pp}i^2_{di}}{CV_{dci}} + \frac{k_pk_{pq}i^2_{qi}}{CV_{dci}}\right)\Delta v_{sdi} + \frac{k_pk_{pp}i_{di}i_{qi} + i_{qi} - k_pk_{pq}i_{di}i_{qi}}{CV_{dci}}\Delta v_{sqi} + \frac{1}{C}\Delta I_{dci} - \frac{k_pk_{pp}i_{di}}{CV_{dci}}\Delta P^*_i - \frac{k_pk_{pq}i_{qi}}{CV_{dci}}\Delta Q^*_i \quad (16)$$

where the linearized form of the auxiliary variables z_{3i} to z_{4i} are:

$$\frac{d\Delta z_{1i}}{dt} = \Delta i^*_{di} - \Delta i_{di} = -(k_{pp}v_{sdi} + 1)\Delta i_{di} - k_{pp}v_{sqi}\Delta i_{qi} + k_{ip}\Delta z_{3i} - k_{pp}i_{di}\Delta v_{sdi} - k_{pp}i_{qi}\Delta v_{sqi} + k_{pp}\Delta P^*_i$$

$$\frac{d\Delta z_{2i}}{dt} = \Delta i^*_{qi} - \Delta i_{qi} = k_{pq}v_{sqi}\Delta i_{di} - (k_{pq}v_{sdi} + 1)\Delta i_{qi} + k_{iq}\Delta z_{4i} - k_{pq}i_{qi}\Delta v_{sdi} + k_{pq}i_{di}\Delta v_{sqi} + k_{pq}\Delta Q^*_i$$

$$\frac{d\Delta z_{3i}}{dt} = \Delta P^*_i - \Delta P_i = v_{sdi}\Delta i_{di} - v_{sqi}\Delta i_{qi} - i_{di}\Delta v_{sdi} - i_{qi}\Delta v_{sqi} + \Delta P^*_i$$

$$\frac{d\Delta z_{4i}}{dt} = \Delta Q^*_i - \Delta Q_i = \Delta Q^*_i + v_{sqi}\Delta i_{di} - v_{sdi}\Delta i_{qi} - i_{qi}\Delta v_{sdi} + i_{di}\Delta v_{sqi}. \quad (17)$$

D. DC NETWORK MODELING

Fig. 4 presents the single line schematic of the MTDC network, where for simplicity the distance (inductance and resistance) of the circuits for all the circuit sections are set identical. DC network dynamics involves with the VSC terminal voltage and the voltage drops through the network resistance and reactance, which can be expressed as:

$$L_{dc}\frac{d}{dt}\begin{bmatrix}\Delta I_{dc1}\\ \Delta I_{dc2}\\ \Delta I_{dc3}\\ \Delta I_{ex}\end{bmatrix} = \begin{bmatrix}\Delta V_{dca} - \Delta V_{dc1} - \Delta I_{dc1}R_{dc}\\ \Delta V_{dc2} - \Delta V_{dca} - \Delta I_{dc2}R_{dc}\\ \Delta V_{dcb} - \Delta V_{dc3} - \Delta I_{dc3}R_{dc}\\ \Delta V_{dca} - \Delta V_{dcb} - \Delta I_{ex}R_{dc}\end{bmatrix} \quad (18)$$

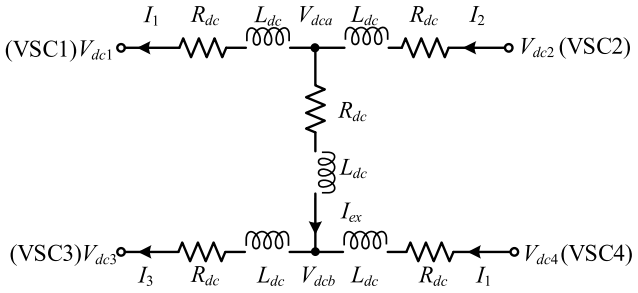

FIGURE 4. Single line schematic of the four-terminal DC network.

where L_{dc} and R_{dc} are the unit line inductance and resistance between any of two adjacent nodes as shown in Fig. 4.

$$I_{ex} = I_{dc2} - I_{dc1} = I_{dc3} - I_{dc4} \quad (19)$$

Substituting (19) into (18), the differential relation of ΔI_{dci} with respect to ΔI_{dci} and ΔV_{dci} can be obtained as

formula (20) by eliminating the internal quantities ΔV_{dca}, ΔV_{dcb}, and ΔI_{ex}.

$$\frac{d}{dt}\begin{bmatrix}\Delta I_{dc1}\\ \Delta I_{dc2}\\ \Delta I_{dc3}\\ \Delta I_{dc4}\end{bmatrix} = \frac{1}{8L_{dc}}\begin{bmatrix}-5 & 3 & 1 & 1\\ -3 & 5 & -1 & -1\\ 1 & 1 & -5 & 3\\ -1 & -1 & -3 & 5\end{bmatrix}\times\begin{bmatrix}\Delta V_{dc1}\\ \Delta V_{dc2}\\ \Delta V_{dc3}\\ \Delta V_{dc4}\end{bmatrix} - \frac{R_{dc}}{L_{dc}}\begin{bmatrix}1 & 0 & 0 & 0\\ 0 & 1 & 0 & 0\\ 0 & 0 & 1 & 0\\ 0 & 0 & 0 & 1\end{bmatrix}\times\begin{bmatrix}\Delta I_{dc1}\\ \Delta I_{dc2}\\ \Delta I_{dc3}\\ \Delta I_{dc4}\end{bmatrix} \quad (20)$$

E. SYSTEM SMALL SIGNAL MODELING

State space equations of VSC subsystems and the integrating DC network are combined to form the mathematical model of the entire system. The small signal model can be obtained by linearization at a predefined operating state as:

$$\Delta\dot{x} = A\Delta x + B\Delta u \quad (21)$$

with Δx being the state vector shown as follows:

$$\Delta x = \begin{bmatrix}\Delta x_1 & \Delta x_2 & \Delta x_3 & \Delta x_4\end{bmatrix}^T$$
$$\Delta x_i = \begin{bmatrix}\Delta i_{di} & \Delta i_{qi} & \Delta V_{dci} & \Delta z_{1i} & \Delta z_{2i} & \Delta z_{3i} & \Delta z_{4i} \times \Delta V_{sdi} & \Delta V_{sqi} & \Delta I_{dci}\end{bmatrix}$$

Δu is the input vector including the input variables which are the reference values of DC voltage, active and reactive power of the four converter stations shown as follows:

$$\Delta u = \begin{bmatrix}\Delta P_1^* & \Delta Q_1^* & \Delta V_{dc2}^* & \Delta P_2^* & \Delta Q_2^* & \Delta P_3^* \times \Delta Q_3^* & \Delta V_{dc4}^* & \Delta Q_4^*\end{bmatrix}^T$$

And A and B are the state and input matrices that can be a function of the steady-state linearization around the initial operating point.

Differential equation (20) combines the state equations of each converter station (as presented in the appendix) to form a 40-dimensional matrix A.

III. ACCURACY VERIFICATION

Before assessing the dynamic stability for the MTDC system, a model verification by comparing with time-domain model is essential to prove the correctness of the mathematical model.

The time-domain model for the candidate MTDC network as presented in Fig. 1 is simulated in Matlab/Simulink. The DC transmission lines are simulated using π-equivalent models with parameters as shown in TABLE 1. The length of the cables is 100 km each. The network and controller parameters in time-domain model are designed in per-unit form as shown in TABLE 2.

TABLE 1. Simulation Parameters [23].

Variables	Value	Variables	Value
Base power	2000MVA	DC link capacitances	500μF
DC grid voltage	500kV	DC cable resistance	13.9mΩ/km
AC voltage	220kV	DC cable capacitance	0.231μF/km
Frequency	50Hz	DC cable inductance	0.159mH/km
SCR	20	X/R	7

TABLE 2. Controller parameters.

controller	value
Inner current controller gains (k_p,k_i)	(0.6,6)
Voltage controller gains (k_{pv},k_{iv})	(2,40)
Active power controller gains (k_{pq},k_{iq})	(1,50)
Reactive power controller gains (k_{pp},k_{ip})	(1,50)
Droop coefficient k_{droop}	2

Small signal analysis is usually carried out around a given steady-state operating point. In this paper the steady operating point of VSCs for all the simulations is set at $V_{dc2} = V_{dc4} = 1$ p.u, $P_1 = -0.2$ p.u, $P_3 = -0.4$ p.u.

The following events are simulated in the sequence as shown in TABLE 3, where common control actions such as active power and DC voltage step changes are included.

TABLE 3. Simulation time sequence.

Time(s)	Event
t=1	P_1^* steps from -0.2 to -0.3 pu
t=2	P_1^* steps from -0.3 to -0.2 pu
t=3	V_{dc4}^* steps from 1 to 0.9 pu
t=4	V_{dc4}^* steps from 0.9 to 0.95 pu

As illustrated in Fig. 5, the simulation response of small signal model as represented by dotted line and the simulation response of the time-domain model as represented by solid line are perfectly matched in overall variation changes with minor differences. This proves that the small signal model would be highly accurate.

IV. STABILITY EVALUATION ON THE MTDC'S DROOP CONTROLLER USING SSSA

A. EIGENVALUES ANALYSIS FUNDAMENTALS

The eigenvalues of the system can be calculated by [17]

$$\det(\lambda I - A) = 0 \quad (22)$$

where I is a diagonal unit matrix with the same dimension as A; λ is the eigenvalue of the system matrix.

The system oscillation modes can be described by its eigenvalues. If all the eigenvalues are located in the left half of the complex plane, the system is stable. When at least one of the eigenvalues has a positive real part, the original system is unstable. The complex eigenvalues always appear

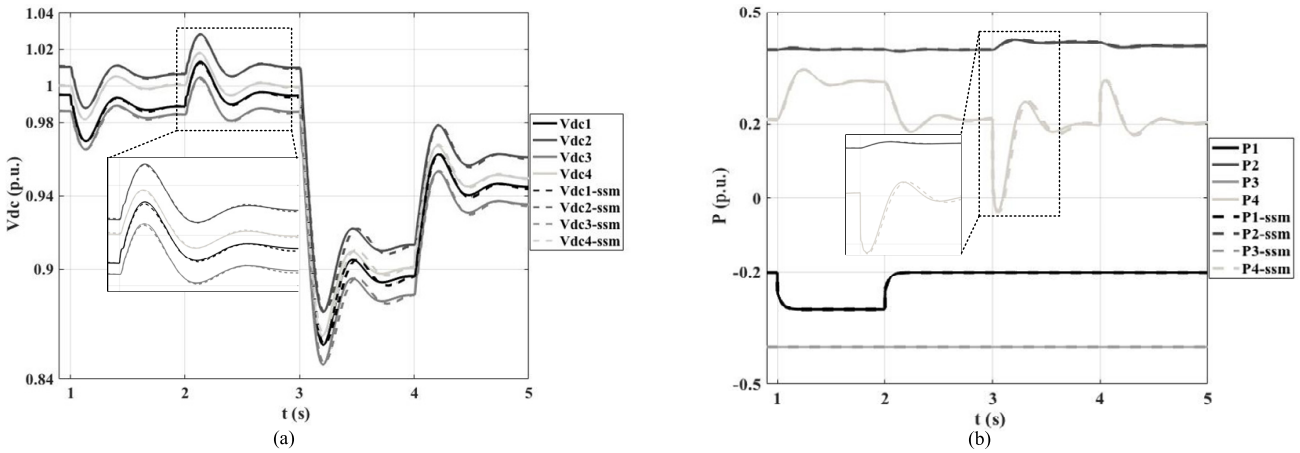

FIGURE 5. Comparison between time-domain model and small signal model: (a) Voltage responses of the four VSCs. (b) Active power responses of the four VSCs.

in conjugate pairs, such as $\lambda_i = \sigma_i \pm j\omega_i$. Each pair of the conjugate eigenvalues corresponds to a certain oscillation mode. The real part σ_i informs the damping characteristic of the system, whereas the imaginary part ω_i informs the oscillation frequency, large ω_i indicates LC resonance and small ω_i indicates low-frequency oscillation.

This paper uses the concept of participation factors to identify the modes representing interactions in the MTDC system by applying the procedure presented in [24]. The impact degree of the eigenvalues on the system states can be estimated by participation factors. The element $P_{ki} = \Phi_{ki}\Psi_{ik}$ is termed the participation factor. Since Φ_{ki} measures the activity of state variable x_k in the ith mode and Ψ_{ik} weighs the contribution of this activity to the mode, the product P_{ki} measures the net participation.

B. EIGENVALUES ANALYSIS

Two types of the prominent eigenvalues should be analyzed: 1) the eigenvalues with real value closest to the imaginary axis, which dominate the system overall response speed; 2) the eigenvalues with obvious imaginary values with respect to their real values, which are linked to poor damping of certain oscillation modes. As observed from TABLE 4 , the pair of eigenvalues $\lambda_{17}\&\lambda_{18}$ are the closest roots to the imaginary axis, which indicate the prominent impact on system stability (with time constant of 1.87 Hz, and 0.46 damping ratio). Also the eigenvalue pairs with large imaginary parts ($\lambda_7\&\lambda_8$, $\lambda_9\&\lambda_{10}$, and $\lambda_{11}\&\lambda_{12}$) are observed, indicating significant poor damping.

The participation factors for the prominent modes as mentioned above are calculated and those with higher impact (higher value) on MTDC system voltage and current are listed in TABLE 5. The participation factor matrix indicates that $\lambda_{17}\&\lambda_{18}$ are related to the DC voltage of the MTDC system and DC voltage integral dynamics Δz_{34}. Please note that Δz_{34} represents the integral part of the DC voltage controller of VSC_4. It can be clearly observed for the prominent oscillation mode of eigenvalue pair $\lambda_{17}\&\lambda_{18}$ that the state variable Δz_{34} of the DC voltage controller integral gains with highest

TABLE 4. Four-terminal system eigenvalues.

λ	Value	Damping ratio	Frequency (Hz)
$\lambda_1\&\lambda_2$	-1226.65±4.34i	1.00	0.69
$\lambda_3\&\lambda_4$	-1221.41±8.33i	0.99	1.33
$\lambda_5\&\lambda_6$	-1215.89±3.99i	1.00	0.63
$\lambda_7\&\lambda_8$	-50.84±**251.84i**	0.19	40.10
$\lambda_9\&\lambda_{10}$	-44.07±**246.96i**	0.18	39.45
$\lambda_{11}\&\lambda_{12}$	-46.49±**174.95i**	0.26	27.97
$\lambda_{13}\&\lambda_{14}$	-26.01±0.40i	0.99	0.099
$\lambda_{15}\&\lambda_{16}$	-25.57±0.37i	0.99	0.10
$\lambda_{17}\&\lambda_{18}$	-4.12±**11.68i**	0.46	1.87
$\lambda_{19}\&\lambda_{20}$	-10.38±0.16i	0.99	0
$\lambda_{21}\&\lambda_{22}$	-10.15±0.41i	0.99	0
$\lambda_{23}\&\lambda_{24}$	-9.80±0.40i	0.99	0
$\lambda_{25}\&\lambda_{26}$	-9.57±0.16i	0.99	0
λ_{27}	-13128.39	1	0
λ_{28}	-584.34	1	0
λ_{29}	-87.42	1	0
λ_{30}	-26.51	1	0
λ_{31}	-25.40	1	0
λ_{32}	-19.10	1	0
λ_{33}-λ_{34}	0	0	0

TABLE 5. Participation factors.

	ΔV_{dc1}	ΔV_{dc2}	ΔV_{dc3}	ΔV_{dc4}	Δz_{34}
$\lambda_{17}\&\lambda_{18}$	0.139	0.135	0.1375	0.1263	**0.528**

participation factor 0.528 plays a dictating role in determining the oscillation characteristics. Nevertheless, the other oscillation modes with higher frequencies may be useful in analyzing and optimizing the power control of the local converters.

C. STABILITY EVALUATION ON THE MTDC's CONTROLLER PARAMETERS

The next step is to analyze the droop coefficient on system stability. As illustrated in pole-zero map of Fig. 6, as k_{droop} varies from 2 p.u to 20 p.u, the system can be maintained stable. The dominate eigenvalue pair $\lambda_{17}\&\lambda_{18}$ move towards the stable region with the decreasing imaginary values and gradually evolve into two decaying modes at $k_{droop} = 18$ where one moves towards the stable region and the other moves towards the unstable region with the damping ratio = 1.

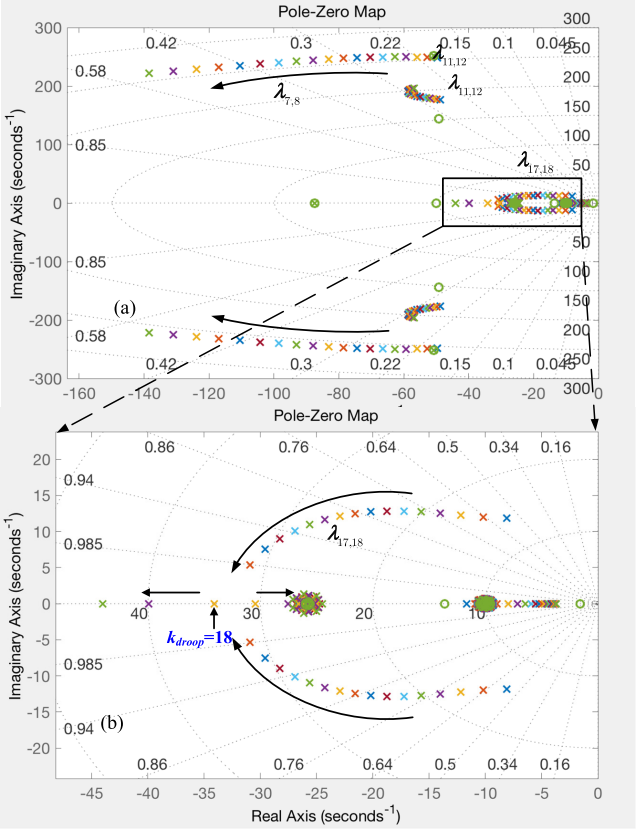

FIGURE 6. Pole-zero map of the multi-terminal dc grid system: (a) The eigenvalue locus when k_{droop} varies from 2 to 20. (b) Magnified view of the eigenvalue locus.

Since the DC voltage controller has great impact on system dynamics, the effect of the proportional and integral gains of the WFVSC DC voltage controllers is investigated.

As shown in Fig. 7, the trajectories of poles and zeroes are generated by varying the proportional gain k_{pv} from 1 p.u to 10 p.u under different droop coefficients (k_{droop} = 2, 10, 20) while keeping the other parameters constant. The poles move towards the stable region with damping ratio getting large, but gradually evolve into two decaying modes with the damping ratio = 1, while one moves towards the stable region the other moves in the opposite direction. Increasing k_{droop} results in more stability which can be seen from the real parts of the eigenvalue pairs.

Similarly, Fig. 8 shows the pole-zero map of the system dynamics when the integral gain k_{iv} varies from 10 p.u to 80 p.u under different droop coefficients (k_{droop} = 2, 10, 20). When k_{droop} = 2, increasing k_{iv} results in higher frequency but less stability which indicates smaller settling time and overshoot. However, when k_{droop} is getting large, the eigenvalues of two decaying modes are combined into one eigenvalue pair with the poles moving to the stable region. Increasing k_{droop} results in more stability and faster speed when the eigenvalues are combined into pairs.

From Fig. 7 and Fig. 8 it can be seen that with large droop coefficient the stability margin is increase and damping ratio can be maintained at 1 in most control parameter combinations, which can be instructive for control parameter selection.

V. SIMULATION

A. VOLTAGE PERFORMANCE UNDER POWER STEP CHANGE

The proposed method for determining the droop coefficient and DC voltage controller gains for stable operation is validated by performing a nonlinear simulation of the network shown in Fig. 1. The wind farm is modeled as equivalent three-phase current sources synchronized with the network frequency. The time-domain simulation in Fig. 9 and Fig. 10 validates the results obtained from the small signal stability analysis. The dynamic responses are analyzed by applying an active power step change in VSC_1 from -0.2 p.u to -0.3 p.u at 2.0 s. To observe the impact of DC voltage gains on voltage stability, three proportional gains (k_{pv} = 2,5,10) and three integral gains (k_{iv} = 20,40,60) were tested for the same step change in power of VSC_2.

It can be seen from Fig. 9 that the variations of k_{pv} influence the states associated with the DC voltage control loops and larger proportional gain of DC voltage controller is beneficial to the stability of DC voltage under different droop coefficients with little overshoot but the settling time is not affected.

From Fig. 10, it can be seen that larger integral gain can effectively shorten the settling time, but at the same time reduce the system damping. According to the requirement of system damping, the appropriate integral gains can be selected by the proposed scheme.

With the increase of droop coefficient, the effect of proportional gain and integral gain is no longer obvious, the overshoot decreases gradually, and the DC voltage tends to be stable. Therefore, the DC voltage controller gains will have little impact on DC voltage with the k_{droop} getting large as a large value of k_{droop} could sufficiently represent steady-state behavior in constant DC voltage control mode.

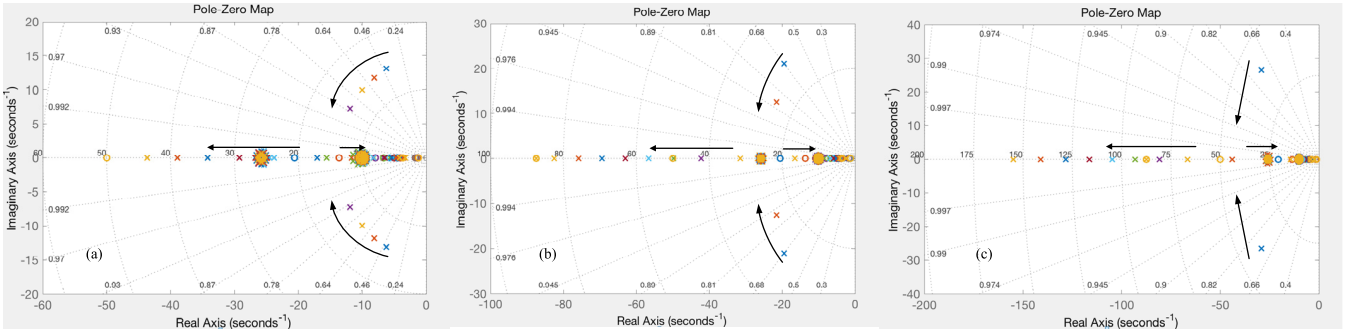

FIGURE 7. Pole-zero map of the multi-terminal dc grid system when k_{pv} varies from 1 to 10: (a) $k_{droop} = 2$. (b) $k_{droop} = 10$. (c) $k_{droop} = 20$.

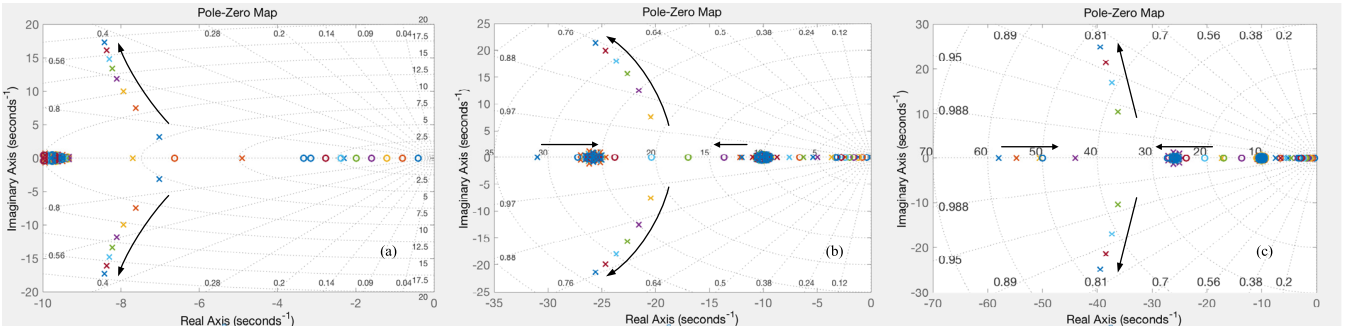

FIGURE 8. Pole-zero map of the multi-terminal dc grid system when k_{iv} varies from 10 to 80: (a) $k_{droop} = 2$. (b) $k_{droop} = 10$. (c) $k_{droop} = 20$.

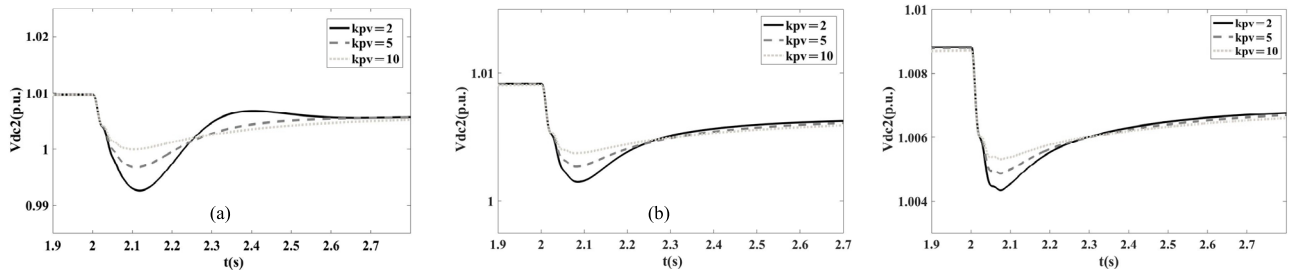

FIGURE 9. DC voltage of the VSC2 with different proportional gains k_{pv}: (a) $k_{droop} = 2$. (b) $k_{droop} = 10$. (c) $k_{droop} = 20$.

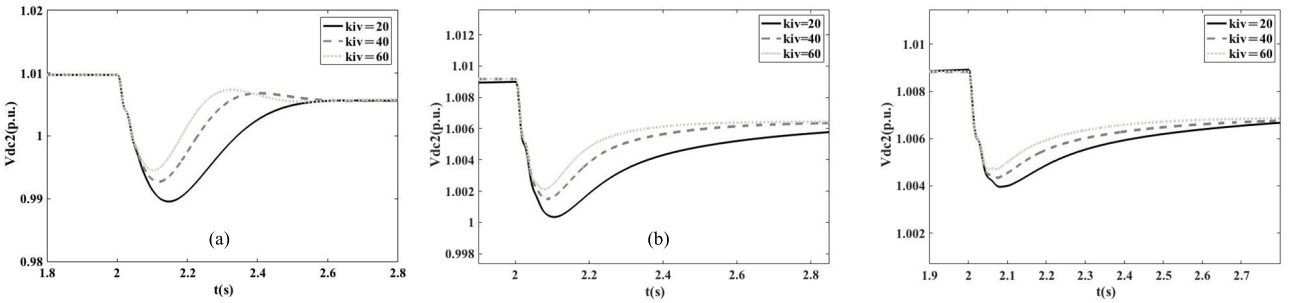

FIGURE 10. DC voltage of the VSC2 with different integral gains k_{iv}: (a) $k_{droop} = 2$. (b) $k_{droop} = 10$. (c) $k_{droop} = 20$.

B. VOLTAGE AND POWER PERFORMANCE UNDER SINGLE-PHASE GIRD FAULT

For further verification on the optimum DC voltage controller gains obtained based on the proposed SSSA method, a single phase-to-ground fault is applied at t = 2s with a fault duration of 0.2 s. As illustrated in the DC voltage chart of Fig. 11 and active power chart of Fig. 12, with $k_{pv} = 10$ the amplitude during the fault can be smaller, and as $k_{iv} = 20$, it leads

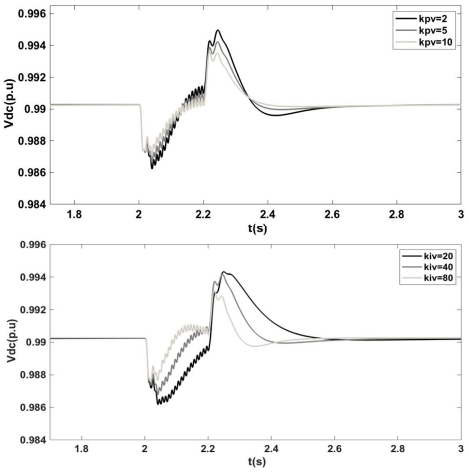

FIGURE 11. DC voltage output of VSC1 with different proportional and integral gains.

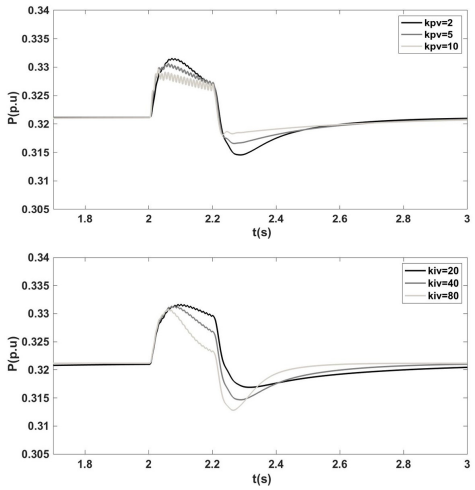

FIGURE 12. Active power output of VSC4 with different proportional and integral gains.

to more damping but slower regulation speed, which validates the results obtained via SSSA. It can be seen that the system remains stable and returns to the pre-fault operating condition soon after the fault is clear. This proves the validity of the approach proposed in this paper. Compared to [10] and [14], the overall SSM of the MTDC system considering

$$
\frac{d}{dt}\begin{bmatrix}
\Delta i_{d1}\\ \Delta i_{q1}\\ \Delta V_{dc1}\\ \Delta z_1\\ \Delta z_2\\ \Delta z_3\\ \Delta z_4\\ \Delta v_{sd1}\\ \Delta v_{sq1}\\ \Delta I_{dc1}
\end{bmatrix}
=
\begin{bmatrix}
-\frac{k_p k_{pp} v_{sd1} + k_p + R}{L} & -\frac{k_p k_{pp} v_{sq1}}{L} & 0 & \frac{k_i}{L} & 0 & \frac{k_p k_{ip}}{L} & 0\\
\frac{k_p k_{pq} v_{sq1}}{L} & -\frac{k_p + R + k_p k_{pq} v_{sd1}}{L} & 0 & 0 & \frac{k_i}{L} & 0 & \frac{k_p k_{iq}}{L}\\
\frac{v_{cd1} + k_p k_{pp} i_{d1} v_{sd1} + k_p i_{d1} - \omega L i_{q1} - k_p k_{pq} v_{sq1} i_{q1}}{C_v V_{dc1}} & \frac{v_{cq1} + \omega L i_{d1} + k_p k_{pp} v_{sq1} i_{d1} + k_p k_{pq} v_{sd1} i_{q1} + k_p i_{q1}}{C_v V_{dc1}} & -\frac{v_{cd1} i_{d1} + v_{cq1} i_{q1}}{C_v V_{dc1}^2} & -\frac{k_i i_{d1}}{C_v V_{dc1}} & -\frac{k_i i_{q1}}{C_v V_{dc1}} & -\frac{k_p k_{ip} i_{d1}}{C_v V_{dc1}} & -\frac{k_p k_{iq} i_{q1}}{C_v V_{dc1}}\\
-(1 + k_{pp} v_{sd1}) & -k_{pp} v_{sq1} & 0 & 0 & 0 & k_{ip} & 0\\
k_{pq} v_{sq1} & -(1 + k_{pq} v_{sd1}) & 0 & 0 & 0 & 0 & k_{iq}\\
-v_{sd1} & -v_{sq1} & 0 & 0 & 0 & 0 & 0\\
v_{sq1} & -v_{sd1} & 0 & 0 & 0 & 0 & 0\\
0 & 0 & 0 & 0 & 0 & 0 & 0\\
0 & 0 & 0 & 0 & 0 & 0 & 0\\
0 & 0 & 0 & 0 & 0 & 0 & 0
\end{bmatrix}
\begin{bmatrix}
\Delta i_{d1}\\ \Delta i_{q1}\\ \Delta V_{dc1}\\ \Delta z_1\\ \Delta z_2\\ \Delta z_3\\ \Delta z_4\\ \Delta v_{sd1}\\ \Delta v_{sq1}\\ \Delta I_{dc1}
\end{bmatrix}
$$

$$
\times
\begin{bmatrix}
-\frac{k_p k_{pp} i_{d1}}{L} & -\frac{k_p k_{pp} i_{q1}}{L} & 0\\
-\frac{k_p k_{pq} i_{q1}}{L} & \frac{k_p k_{pq} i_{d1}}{L} & 0\\
\frac{i_{d1} + k_p k_{pp} i_{d1}^2 + k_p k_{pq} i_{q1}^2}{C_v V_{dc1}} & \frac{i_{q1} + k_p k_{pp} i_{d1} i_{q1} - k_p k_{pq} i_{d1} i_{q1}}{C_v V_{dc1}} & \frac{1}{C_v}\\
-k_{pp} i_{d1} & -k_{pp} i_{q1} & 0\\
-k_{pq} i_{q1} & k_{pq} i_{d1} & 0\\
-i_{d1} & -i_{q1} & 0\\
-i_{q1} & i_{d1} & 0\\
0 & 0 & 0\\
0 & 0 & 0\\
0 & 0 & 0
\end{bmatrix}
\times
\begin{bmatrix}
\Delta i_{d1}\\ \Delta i_{q1}\\ \Delta V_{dc1}\\ \Delta z_1\\ \Delta z_2\\ \Delta z_3\\ \Delta z_4\\ \Delta v_{sd1}\\ \Delta v_{sq1}\\ \Delta I_{dc1}
\end{bmatrix}
+
\begin{bmatrix}
\frac{k_p k_{pp}}{L} & 0\\
0 & \frac{k_p k_{pq}}{L}\\
-\frac{k_p k_{pp} i_{d1}}{C_v V_{dc1}} & -\frac{k_p k_{pq} i_{q1}}{C_v V_{dc1}}\\
k_{pp} & 0\\
0 & k_{pq}\\
1 & 0\\
0 & 1\\
0 & 0\\
0 & 0\\
0 & 0
\end{bmatrix}
\times
\begin{bmatrix}
P_1^*\\ Q_1^*
\end{bmatrix}
$$

$$
\frac{d}{dt}\begin{bmatrix}\Delta i_{di}\\ \Delta i_{qi}\\ \Delta V_{dci}\\ \Delta z_{1i}\\ \Delta z_{2i}\\ \Delta z_{3i}\\ \Delta z_{4i}\\ \Delta v_{sdi}\\ \Delta v_{sqi}\\ \Delta I_{dci}\end{bmatrix}
=\begin{bmatrix}
-\frac{k_p+R_c+k_pk_{pv}v_{sdi}}{L_c} & -\frac{k_pk_{pv}v_{sqi}}{L_c} & -\frac{k_pk_{pv}k_{droop}}{L_c} & \frac{k_i}{L_c} & 0\\
\frac{k_pk_{pq}v_{sqi}}{L} & -\frac{k_p+R+k_pk_{pq}v_{sdi}}{L} & 0 & 0 & \frac{k_i}{L_c}\\
\frac{v_{cdi}+k_pi_{di}+k_pk_{pv}i_{di}v_{sdi}-\omega L_ci_{qi}-k_pk_{pq}i_{qi}v_{sqi}}{C_vV_{dci}} & \frac{v_{cqi}+k_pi_{qi}+\omega Li_{di}+k_pk_{pv}i_{di}v_{sq}+k_pk_{pq}i_{qi}v_{sdi}}{C_vV_{dci}} & -\frac{(v_{cdi}i_{di}+v_{cqi}i_{qi})}{C_vV_{dci}^2}+\frac{k_pk_{pv}k_{droop}i_{di}}{C_vV_{dci}} & -\frac{k_ii_{di}}{C_vV_{dci}} & -\frac{k_ii_{qi}}{C_vV_{dci}}\\
-(k_{pv}v_{sdi}+1) & -k_{pv}v_{sqi} & -k_{pv}k_{droop} & 0 & 0\\
k_{pq}v_{sqi} & -(1+k_{pq}v_{sdi}) & 0 & 0 & 0\\
-v_{sdi} & -v_{sqi} & -k_{droop} & 0 & 0\\
v_{sqi} & -v_{sdi} & 0 & 0 & 0\\
0 & 0 & 0 & 0 & 0\\
0 & 0 & 0 & 0 & 0\\
0 & 0 & 0 & 0 & 0
\end{bmatrix}
\begin{bmatrix}
\frac{k_pk_{iv}}{L_c} & 0 & -\frac{k_pk_{pv}i_{d2}}{L_c} & -\frac{k_pk_{pv}i_{q2}}{L_c} & 0\\
0 & \frac{k_pk_{iq}}{L_c} & -\frac{k_pk_{pq}i_{qi}}{L} & \frac{k_pk_{pq}i_{di}}{L} & 0\\
-\frac{k_pk_{iv}i_{di}}{C_vV_{dci}} & -\frac{k_pk_{iq}i_{qi}}{C_vV_{dci}} & \frac{k_pk_{pv}i_{di}^2+k_pk_{pq}i_{qi}^2}{CV_{dci}} & \frac{k_pk_{pv}i_{di}i_{qi}+i_{qi}-k_pk_{pq}i_{di}i_{qi}}{CV_{dci}} & -\frac{1}{C_v}\\
k_{iv} & 0 & -k_{pv}i_{di} & -k_{pv}i_{qi} & 0\\
0 & k_{iq} & -k_{pq}i_{qi} & k_{pq}i_{di} & 0\\
0 & 0 & -i_{di} & -i_{qi} & 0\\
0 & 0 & -i_{qi} & i_{di} & 0\\
0 & 0 & 0 & 0 & 0\\
0 & 0 & 0 & 0 & 0\\
0 & 0 & 0 & 0 & 0
\end{bmatrix}
\times\begin{bmatrix}\Delta i_{di}\\ \Delta i_{qi}\\ \Delta V_{dci}\\ \Delta z_{1i}\\ \Delta z_{2i}\\ \Delta z_{3i}\\ \Delta z_{4i}\\ \Delta v_{sdi}\\ \Delta v_{sqi}\\ \Delta I_{dci}\end{bmatrix}
+\begin{bmatrix}
\frac{k_pk_{pv}k_{droop}}{L_c} & \frac{k_pk_{pv}}{L_c} & 0\\
0 & 0 & \frac{k_pk_{pq}}{L}\\
-\frac{k_pk_{pv}k_{droop}i_{di}}{CV_{dci}} & -\frac{k_pk_{pv}i_{di}}{CV_{dci}} & -\frac{k_pk_{pq}i_{qi}}{CV_{dci}}\\
k_{pv}k_{droop} & k_{pv} & 0\\
0 & 0 & k_{pq}\\
k_{droop} & 1 & 0\\
0 & 0 & 1\\
0 & 0 & 0\\
0 & 0 & 0\\
0 & 0 & 0
\end{bmatrix}
\times\begin{bmatrix}\Delta V_{dci}^*\\ \Delta P_i^*\\ \Delta Q_i^*\end{bmatrix}
$$

DC network electrical dynamics can be obtained and the accuracy can be guaranteed.

VI. CONCLUSION

In this paper, a small-signal model of VSC-HVDC system is established for transient stability analysis, in which subsystems of converter stations are interconnected by DC network model of differential equations. Based on this model, the small-signal stability of the system is analyzed and a selection criterion for the droop controller is provided. A comparison of the system performance with different droop coefficients and DC voltage controller gains has been shown. The validity of derived small signal model was demonstrated by the good agreement between results from using

the proposed method and the corresponding time-domain simulation results applied to a four-terminal MTDC network.

Based on this model, the small signal stability analysis is carried out to evaluate the impact of DC voltage controller parameters on DC network voltage stability, and the comparisons of the system performance with various droop coefficients and DC voltage controller gains have been undertaken. An important generic stability evaluation method using the derived small signal model is then raised to ensure the MTDC system stability without considering time-domain models. However, to facilitate analysis the wind farm is simplified in the process of modeling, but there will be slight deviation from the actual results in the parameters of model controller. Future work will continue to improve this field.

APPENDIX

small signal model of constant active power converter station, equation shown at the bottom of the tenth page, small signal model of DC voltage droop converter station, equation shown at the top of the previous page.

REFERENCES

[1] N. Flourentzou, V. G. Agelidis, and G. D. Demetriades, "VSC-based HVDC power transmission systems: An overview," *IEEE Trans. Power Electron.*, vol. 24, no. 3, pp. 592–602, Mar. 2009.

[2] J. Lv, P. Dong, G. Shi, X. Cai, H. Rao, and J. Chen, "Subsynchronous oscillation of large DFIG-based wind farms integration through MMC-based HVDC," in *Proc. Int. Conf. Power Syst. Technol.*, Chengdu, China, Oct. 2014, pp. 2401–2408.

[3] H. Liu and J. Sun, "Voltage stability and control of offshore wind farms with AC collection and HVDC transmission," *IEEE J. Emerg. Sel. Topics Circuits Syst.*, vol. 2, no. 4, pp. 1181–1189, Dec. 2014.

[4] M. Cheah-Mane, L. Sainz, J. Liang, N. Jenkins, and C. E. Ugalde-Loo, "Criterion for the electrical resonance stability of offshore wind power plants connected through HVDC links," *IEEE Trans. Power Syst.*, vol. 32, no. 6, pp. 4579–4589, Nov. 2017.

[5] G. Pinares, L. B. Tjernberg, L. A. Tuan, C. Breitholtz, and A.-A. Edris, "On the analysis of the DC dynamics of multi-terminal VSC-HVDC systems using small signal modeling," in *Proc. IEEE Grenoble Conf.*, Grenoble, France, Jun. 2013, pp. 1–6.

[6] N. R. Chaudhuri and B. Chaudhuri, "Adaptive droop control for effective power sharing in multi-terminal DC (MTDC) grids," in *Proc. IEEE Power Energy Soc. Gen. Meeting*, Vancouver, BC, Canada, Jul. 2013, p. 1.

[7] L. Zhang, L. Harnefors, and H.-P. Nee, "Interconnection of two very weak AC systems by VSC-HVDC links using power-synchronization control," *IEEE Trans. Power Syst.*, vol. 26, no. 1, pp. 344–355, Feb. 2011.

[8] M. Raza, E. Prieto-Araujo, and O. Gomis-Bellmunt, "Small-signal stability analysis of offshore AC network having multiple VSC-HVDC systems," *IEEE Trans. Power Del.*, vol. 33, no. 2, pp. 830–839, Apr. 2018.

[9] D. Dong, B. Wen, D. Boroyevich, P. Mattavelli, and Y. Xue, "Analysis of phase-locked loop low-frequency stability in three-phase grid-connected power converters considering impedance interactions," *IEEE Trans. Ind. Electron.*, vol. 62, no. 1, pp. 310–321, Jan. 2015.

[10] J. Z. Zhou, H. Ding, S. Fan, Y. Zhang, and A. M. Gole, "Impact of short-circuit ratio and phase-locked-loop parameters on the small-signal behavior of a VSC-HVDC converter," *IEEE Trans. Power Del.*, vol. 29, no. 5, pp. 2287–2296, Oct. 2014.

[11] W. Du, Q. Fu, X. Wang, and H. F. Wang, "Small-signal stability analysis of integrated VSC-based DC/AC power systems–a review," *Int. J. Electr. Power Energy Syst.*, vol. 103, pp. 545–552, Dec. 2018.

[12] G. B. Diaz, J. A. Suul, and S. D'Arco, "Small-signal state-space modeling of modular multilevel converters for system stability analysis," in *Proc. IEEE Energy Convers. Congr. Expo. (ECCE)*, Montreal, QC, Canada, Sep. 2015, pp. 5822–5829.

[13] Y. Yuan, C. Zhao, B. Yuan, and J. Xu, "Analysis and optimization of reactive power controllers of voltage source converter in weak AC grid," *Power Syst. Technol.*, vol. 40, no. 3, pp. 697–703, Mar. 2016.

[14] G. O. Kalcon, G. P. Adam, O. Anaya-Lara, S. Lo, and K. Uhlen, "Small-signal stability analysis of multi-terminal VSC-based DC transmission systems," *IEEE Trans. Power Syst.*, vol. 27, no. 4, pp. 1818–1830, Nov. 2012.

[15] Y. Huang, A. Tang, B. Xiong, Y. Huang, H. Tang, and Y. Li, "Modelling of multi-VSCs in DC voltage control timescale for small-signal stability analysis," *J. Eng.*, vol. 2017, no. 13, pp. 2057–2061, 2017.

[16] T. M. Haileselassie and K. Uhlen, "Impact of DC line voltage drops on power flow of MTDC using droop control," *IEEE Trans. Power Syst.*, vol. 27, no. 3, pp. 1441–1449, Aug. 2012.

[17] D. N. Huu, "Small signal assessment of an AC system integrated with a VSC-HVDC network," in *Proc. IEEE EUROCON*, Salamanca, Spain, Sep. 2015, pp. 1–6.

[18] L. Xu and L. Yao, "DC voltage control and power dispatch of a multi-terminal HVDC system for integrating large offshore wind farms," *IET Renew. Power Gener.*, vol. 5, no. 3, pp. 223–233, May 2011.

[19] W. Li, Y. Che, C. Hong, Y. Zhang, and J. Yang, "VSC-MTDC droop control strategy considering transmission loss and renewable energy fluctuation," *Electr. Power Automat. Equip.*, vol. 37, no. 8, pp. 220–226, Aug. 2017.

[20] Y. A.-R. I. Mohamed and E. F. El-Saadany, "Adaptive decentralized droop controller to preserve power sharing stability of paralleled inverters in distributed generation microgrids," *IEEE Trans. Power Electron.*, vol. 23, no. 6, pp. 2806–2816, Nov. 2008.

[21] J. Beerten, S. D'Arco, and J. A. Suul, "Identification and small-signal analysis of interaction modes in VSC MTDC systems," in *Proc. IEEE Power Energy Soc. Gen. Meeting (PESGM)*, Boston, MA, USA, Jul. 2016, p. 1.

[22] L. Xiao, Z. Xu, T. An, and Z. Bian, "Improved analytical model for the study of steady state performance of droop-controlled VSC-MTDC systems," *IEEE Trans. Power Syst.*, vol. 32, no. 3, pp. 2083–2093, May 2017.

[23] A. Kirakosyan, E. F. El-Saadany, M. S. E. Moursi, and K. A. Hosani, "DC voltage regulation and frequency support in pilot voltage droop-controlled multiterminal HVDC systems," *IEEE Trans. Power Del.*, vol. 33, no. 3, pp. 1153–1164, Jun. 2018.

[24] J. Beerten, G. B. Diaz, and S. D'Arco, and J. A. Suul, "Comparison of small-signal dynamics in MMC and two-level VSC HVDC transmission schemes," in *Proc. IEEE Int. Energy Conf. (ENERGYCON)*, Leuven, Belgium, Apr. 2016, pp. 1–6.

YANBO CHE was born in Shandong, China. He received the B.S. degree from Zhejiang University, Hangzhou, China, in 1993, and the M.S. and Ph.D. degrees from Tianjin University, Tianjin, China, in 1996 and 2002, respectively, where he is currently an Associate Professor with the School of Electrical and Information Engineering. Since 1996, he has been engaged in teaching and scientific research of power electronic technology and power systems His current research interests include power electronics, renewable energy resources, and micro-grids.

JINGJING JIA was born in Hebei, China. She received the B.S. degree from Northwestern Polytechnical University, Xi'an, China, in 2017. She is currently pursuing the M.S. degree with Tianjin University, Tianjin, China. Her current research interests include power electronics and stability analysis of HVDC transmission systems.

JIEBEI ZHU received the B.S. degree in microelectronics from Nankai University, Tianjin, China, in 2008, and the M.Sc. and Ph.D. degrees in electronic and electrical engineering from the University of Strathclyde, Glasgow, U.K., in 2009 and 2013, respectively. Since 2013, he has been a Senior Power System Engineer and an Innovation Project Manager with National Grid Plc. of the GB transmission system operator. He successively chairs the modeling project of GB Electricity Ten Year Statement, guides HVDC network developments in North Sea for the EU project of European Ten Year Network Development Plan, and advises system operations and security for Scotland in real time for the GB Electricity Network Control Center. He is currently supported by 1000 Young Talents program by the China Central Organization Committee, as a Full Professor with the School of Electrical Automation and Information Engineering, Tianjin University. His research interests include HVDC transmission system control, renewable energy systems, and energy storage technologies. He received the license of Chartered Engineer by U.K. Engineering Council and IET.

XIALIN LI, photograph and biography not available at the time of publication.

ZIHAN LV was born in Anhui, China. She received the B.S. degree from the Anhui University of Science & Technology, Huainan, China, in 2018. She is currently pursuing the M.S. degree with Tianjin University, Tianjin, China. Her current research interests include power electronics, HVDC transmission system control, and renewable energy resources.

MING LI, photograph and biography not available at the time of publication.